High order harmonic generation on solid target

7.1 Introduction

In this chapter, after an historical overview of the high harmonic generation (HHG) on solid targets, I give a theoretical introduction of the two harmonic generation mechanisms and of the possibility of obtaining attosecond pulses from these harmonics. I then introduce the plasma mirror interaction regime that occurs for intensities below the generation of harmonics. This plasma mirror interaction can be used to increase the temporal contrast of the laser pulses. The first experiments of laser-matter interaction in this regime are presented in the last section.

7.2 Historical overview

High harmonic generation from solid plasmas was first observed by using high-energy nanosecond pulses from CO_2 laser systems [5, 6, 7]. In these experiments pulses with an energy in the Joule level at 10.6 μJ with ns duration were focused to the intensity of $\backsim 10^{15}\ Wcm^{-2}$, and harmonics up to 46th order ($\backsim 230\ nm$) were observed. Theoretical studies attributed the harmonic generation mechanism to the nonlinear restoring force of the plasma and mode coupling into plasma oscillations [2]. They also predicted that there would be a cut-off in the harmonic spectrum, whose position is determined by the plasma density. Another decade was needed until the first observation of harmonics from plasma surfaces using femtosecond pulses produced by table-top Ti:Sapphire laser systems [25]. Typical parameters were $\backsim 100mJ$ of energy at $\backsim 800nm$ with $\backsim 100fs$ duration. Although the pulse energy was 3 orders of magnitude lower than that from CO_2 lasers, the pulse duration, being shorter by 4 orders of magnitude, allowed to achieve the intensity of $\backsim 10^{17}Wcm^{-2}$. On the other hand, since the relativistic amplitude scales as $a_L^2 \propto I\lambda^2$, higher intensity was compensated by shorter wavelength, i.e., the value of a_L was comparable to that of CO_2 lasers. Nevertheless, it was shown that surface harmonics can be generated with a much smaller, table top laser system. In the meanwhile, numerical simulations (particle-in-cell PIC simulation code) found that there is no cut-off in

the spectrum [10], which is in contrast with the prediction from previous studies. Harmonics beyond the predicted cut-off were also experimentally observed using a high power, picosecond Nd:glass laser with a focal intensity of $\backsim 10^{19} W cm^{-2}$ at 1053 nm [18]. A new theoretical model was proposed to explain these results, which is known as the oscillating mirror model [14]. The model predicts that the harmonics are generated from fast moving reflective surface [4]. The appearance of the cut-off in the previous mode-coupling picture was attributed to the low resolution PIC simulations [10]. The oscillating mirror model and the numerical simulations predicted that the harmonic generation could be extended well beyond the previously expected cut off by increasing the laser intensity to the relativistic regime [10]. This new prediction leads to growing interest into harmonic generation from plasma surfaces as a source of coherent XUV radiation. Many experimental studies have followed. Several investigations have found that the harmonic generation process is strongly dependent on the plasma scale length [26, 22]. Harmonic generation efficiency was found to have an optimal scale length above zero, and then drop rapidly as the scale length increases [26, 12]. In fact, improving the temporal contrast of the incident pulses was found to be beneficial to the harmonics generation process [15]. Angular distribution of the generated harmonics was also studied. For picosecond laser pulses, the angular distribution was found to be near isotropic rather than specular [18], which was attributed to surface rippling owing to the high ponderomotive pressure. On the other hand, XUV beam directed in the specular direction was observed for femtosecond laser pulses [22], where the interaction occurs faster than the plasma expands. The polarization dependence of the process was studied by several group [18, 22]. The harmonic generation efficiency was observed to be lower for s-polarization when femtosecond pulses were used [26, 22], which was consistent with the prediction of the oscillating-mirror model [14].

Theoretical work has pursued the possibility of the harmonic generation process as a source of attosecond pulses. It was pointed out that harmonics are inherently phase locked and that leads to a train of attosecond pulses [19]. Another work proposed to focus a few-cycle pulse into a spot as small as the fundamental wavelength (λ^3), which leads to the generation of an isolated single attosecond pulse in a certain direction [16]. Analytical work similar to the oscillating-mirror model [11] has revealed that the harmonics spectra scales as a power law: $I_q \propto q^{-p}$, where q is the harmonic order and p is the scaling parameter p$\backsim$ 2.5. From this slow power-law decay, they predicted that even a train of zeptosecond pulses could be produced. This scaling was verified by experimental observation of the harmonic spectrum scaling law. It was also predicted that the cut-off position should scale as $\backsim \gamma^3$, where γ is the relativistic γ-factor. This means that the highest harmonics generated from this process scales up very rapidly when the intensity of the incident field is increased. This scaling of the cut-off was also confirmed experimentally [8]. One more important thing to be mentioned are the studies on of harmonic generation in non relativistic regime [20]. They found that there is a harmonic generation process efficient with non-relativistic intensity, which they named as coherent wake emission (CWE). The results predicted from their model are similar to the prediction from very early theoretical models, for example, the observation of the cut-off.

7.3 Harmonic generation mechanism

Harmonic generation mechanism from solid surfaces is categorized into two different regimes depending on the incident laser intensity: relativistic regime and non-relativistic regime. The former is known as relativistic oscillating mirror (ROM) model [14, 25], while the latter is named as coherent wake emission (CWE) [20].

7.3.1 Relativistic oscillating mirror

To understand the physical mechanism of harmonic generation from solid target, we can consider an electromagnetic wave incident on the surface composed of a number of electrons that can oscillate around an immovable ion background (Fig. 7.1). The plasma can be directly created from the solid target by the leading edge of the laser pulse. The plasma electrons are accelerated along the polarization direction by the electric field and acquire a velocity that is proportional to the normalized filed amplitude a_L:

$$a_L = \frac{eE_L}{\omega_L mc} \tag{7.1}$$

where E_L and ω_L are the electric field and the laser frequency respectively. As long as the laser intensity is such that $a_L << 1$, the magnetic field B does not play any relevant role, but it becomes relevant for $a_L \geq 1$. In such condition the Lorentz force $F_p \propto \overrightarrow{B} \backsim I_L \lambda_L^2 sin(2\omega_L t)$ tends to move the electrons parallel to the laser propagation direction inducing an oscillatory motion. The interplay between the Lorentz force and the restoring force due to the electrostatic field induced charge separation, determines an oscillatory motion. Since the incident electromagnetic pulse is reflected at the electron surface and this surface is moving relativistically, the incident field experience an extreme Doppler up shift up to:

$$\Omega_{max} \approx 4\gamma_{max}^2 \omega_L = 4(1 + a_L^2)\omega_L \tag{7.2}$$

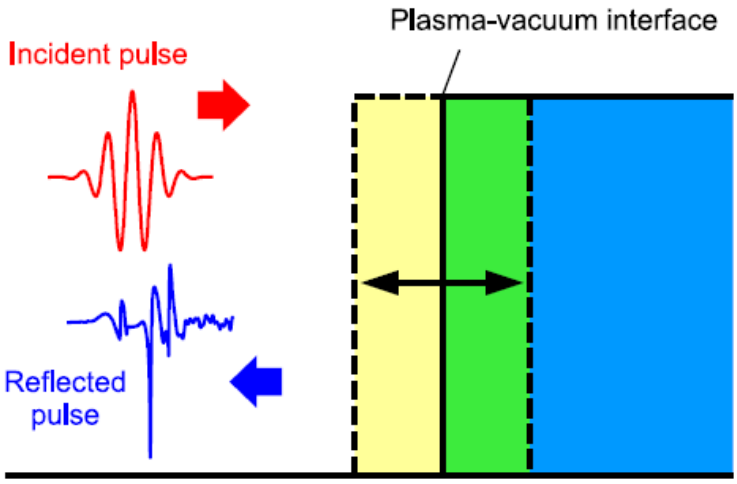

Figure 7.1: Schematic drawing of oscillating mirror. The electromagnetic field of the incident pulse drives the plasma-vacuum interface back and forth. The pulse experience a huge Doppler shift upon reflection on the oscillating surface, which leads to the generation of high frequency components. Reprinted from [17]

7.3.2 The relativistic γ-spikes model

The oscillating mirror model offers a simple and intuitive picture of the harmonic generation process for solids, leading to a simple law for the cut-off frequency. However, recent experimental works have evidenced a different evolution of the cut-off frequency as a function of the maximum relativistic γ_{max}. The experimental data have been interpreted using a different theoretical analysis performed by Baeva et al.[1]. This theory allows one to recognize the different behavior between the plasma electrons and the plasma surface during the interaction with the relativistic laser pulse. Indeed, whereas the velocity of the electrons are close to the speed of light in all instants (with a component both normal p_n and parallel p_τ to the plasma surface), the plasma boundary behave in a quite different way. Its velocity v_s is not ultra-relativistic for most of the times but smoothly approaches c only when the tangential electron momentum vanishes (Fig. 7.2(a),(b)). The γ-factor of the surface γ_s also shows a specific behavior Fig. 7.2(c). It has sharp peaks at those times for which the velocity of the surface approaches c. Thus, while the velocity function v_s is characterized by its smoothness, the distinctive feature of γ_s are its quasi-singularities. When v_s reaches its maximum and γ_s has a sharp peak, high harmonics of the incident wave are generated and can be seen in the reflected radiation. The temporal width of this γ spike scale as $\Delta t \sim 1/\gamma_{max}$. In other words the duration of the emitted pulse scales accordingly. Since this pulse is compressed by Doppler shift by a factor $4\gamma_{max}^2$ and the emission of these harmonics is confined to a time interval $\Delta t/4\gamma_{max}^2 \sim 1/\gamma_{max}^3$ it thus contains frequencies up to $\sim \gamma_{max}^3$. This theoretical prediction is in agreement with experimental results. In particular it demonstrates way a universal harmonic spectrum (that does not depend on the particular surface motion) can be derived. Physically, only the time interval of γ-spiking is

responsible for harmonic generation. Consequently only region around the maximum velocity v_s corresponds to the harmonic spectrum. As a result, since all smooth functions resemble parabolas around their maxima, the harmonic spectrum is universal (Fig. 7.3). It contains two qualitatively different parts: a power low decay (to the spectral cut-off) and an exponential decay.

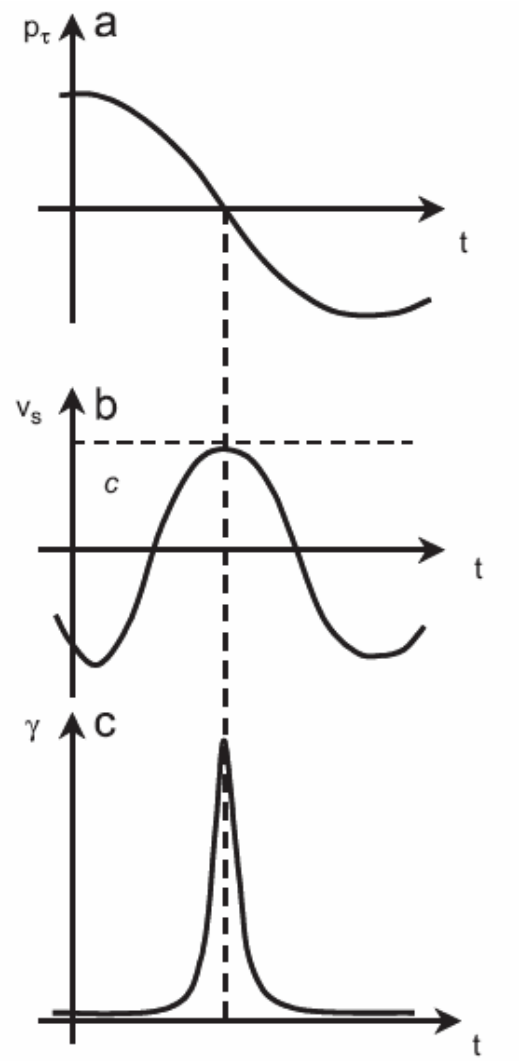

Figure 7.2: Schematic view of the principle of the γ spike model. (a) Electron momentum component parallel to the surface as a function of time; (b) velocity of the plasma surfaces and (c) γ factor of the surface. Reprinted from [1].

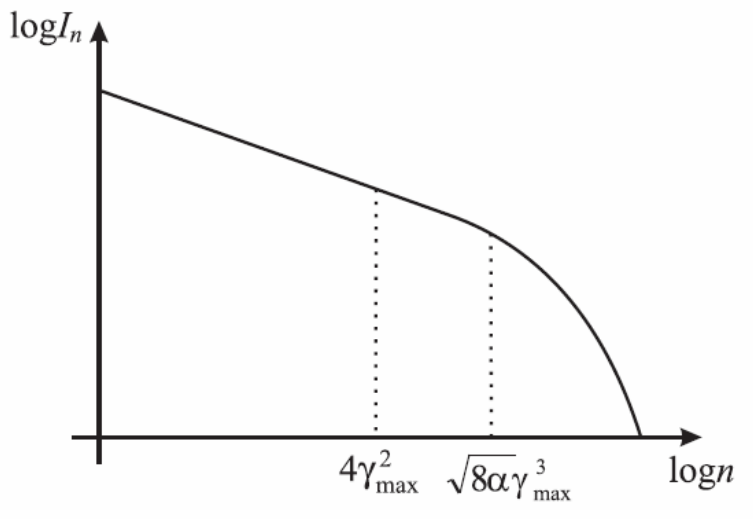

Figure 7.3: The universal high harmonic spectrum contains power law decay and exponential decay (plotted in log-log scale).

7.3.3 Coherent wake emission

When the intensity of the incident laser field is not relativistic,the oscillating mirror does not generate harmonic efficiently and CWE becomes dominant. Fig. 7.4 illustrates the process of CWE. The CWE is a process associated with plasma wake oscillation. This process occurs for a p-polarized incident electric field. When a pulse is incident on the surface of the plasma, the electric field of the pulse pulls electrons out from the plasma. Those electrons, named Brunel electrons, are driven back into the plasma by the same electric field and absorbed by the plasma, a process known as vacuum heating [3]. These electrons bunch in the plasma density gradient and constitute a density wave inside the plasma. As the density wave travels, it triggers plasma oscillations in its wake. These plasma oscillations are converted back to electromagnetic waves at the point where the wave front of the wake turn around [21]. As the generated electromagnetic wave travels along the density gradient, it refracts and comes out of the plasma in the specular direction of the incident beam. Since this occur within a fraction of cycle, each wave generated is in a form of a pulse shorter than one optical cycle, possibly sub-femtosecond. The CWE process has several interesting properties. As apposed to the ROM harmonic generation, this process is efficient down to the incident intensity of $I\lambda^2 \sim 4 \times 10^{15} W cm^{-2}$ [20], which corresponds to the normalized amplitude of $a_L \sim 0.05$. Therefore, CWE will be the dominant harmonic generation mechanism when the intensity is non relativistic. Another important feature of CWE is that the harmonic spectra shows a clear cut-off at the maximum plasma frequency ω_p, which is determined by the density of the plasma. The reason way no harmonics are generated above ω_p, is that the generation process relies on the density wave in the plasma. This is in contrast with the spectra of ROM harmonics, where it shows a slow roll-over around the frequency $\sqrt{8}\gamma^3_{max}$. The harmonics and a pulse train generated from CWE is chirped in two ways. One is a chirp generated within the density

gradient, because the higher frequency component is generated from the higher-density part in the plasma and hence needs to travel more to come out of the plasma. The other is a chirp coming from the velocity of the electrons pulled out into the vacuum. Since the velocity of the electrons is dependent on the intensity of the incident pulse, the time they require to re-collide with the plasma surface depends on the intensity. In other words it gains a chirp according to the intensity envelope of the pulse. The former introduces a chirp in a single attosecond pulse in a train, which is analogous to an chirp observed in gas HHG [24], while the latter changes the time spacing between individual pulses in a train, analogous to a harmonic chirp [24]. A typical CWE spectrum is shown in Fig. 7.5.

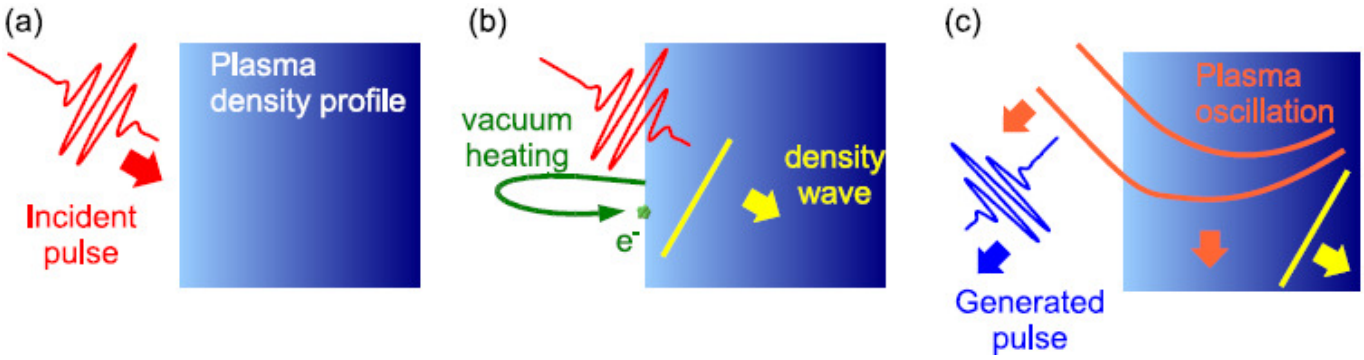

Figure 7.4: Schematic illustration of the coherent wake emission. (a) The pulse enter the plasma density gradient with an oblique incidence. (b) The electric field of the pulse pulls electrons out from the plasma into the vacuum and then drives them back into the plasma. The plasma gains the energy through the recollision (vacuum heating) and plasma density wave is generated. (c) Plasma oscillation in the wake of the density wave generates a pulse back into the vacuum. Reprinted from [17]

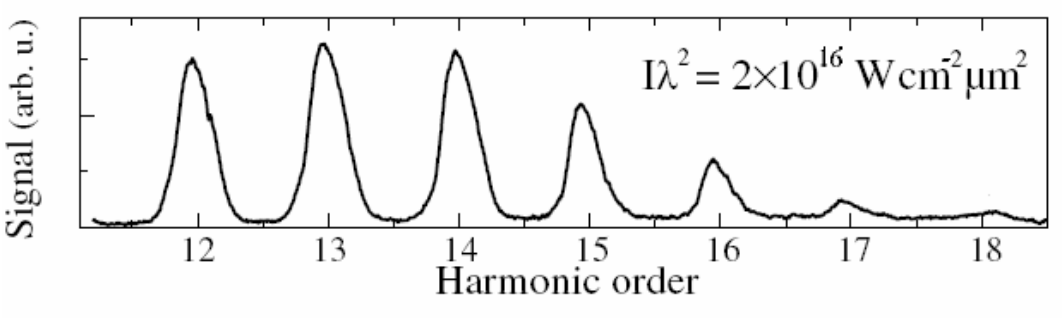

Figure 7.5: Typical raw harmonic spectrum

7.4 Route to intense attosecond pulses

One of the most appealing aspects of harmonic generation from solid surfaces is its potential to generate intense attosecond pulses [23]. In fact the predicted harmonic generation efficiency is several order of magnitude higher than that of gas HHG and thus attosecond with very high intensity are expected. According to theoretical studies, the surface HHG process is capable of generating a train of attosecond pulses [19] or an isolated attosecond pulse [23, 16].

7.4.1 Generation of a train of attosecond pulses

When several equidistant frequencies are phase-locked, superposing them will lead to a train of pulses much shorter than the cycle of the original frequencies. Applying this idea to the harmonics was proposed to generate a train of attosecond pulses [9]. One of the properties that makes harmonic generation process suitable for attosecond pulse generation is its broad spectral span of the generated harmonics. Even for harmonics from a monochromatic wave, the overall spectral bandwidth is as wide as $\triangle\omega \backsim 2N\omega$, where N is the number of the synthesized harmonics. The expected pulse duration after the Fourier synthesis is $\tau \backsim 1/\triangle\omega \backsim 1/2N\omega$. Note that the factor of 2 appears only for gas HHG, where only odd harmonics are generated. For example, when a 800 nm fundamental wave ($\omega = 2.35 \times 10^{15} Hz$) is used, synthesizing three harmonic of gas HHG (five for surface HHG) can lead to an attosecond pulse train, where each pulse is as short as $\sim 100as$. Above mentioned analysis assumed that the harmonics were phase locked which is not necessary the case in reality. In fact, it was found that the

individual atoms are not phase locked in the gas HHG process. On the other hand it was also found that the propagation in the atomic media will results in the phase locking of the harmonics, which allows the generation of a attosecond pulse train. This have been successfully experimentally demonstrated. Since the physical origin of harmonic generation from plasma surfaces is different from that of gas HHG, the same question arise as whether harmonics are phase locked and attosecond pulses can really be generated. Theoretical studies found that this is indeed the case and predicted that it is possible to generate a train of attosecond pulses [19].

7.4.2 Generation of isolated attosecond pulses

Although a train of attosecond pulses can be used for applications such as spectroscopy, the interpretation of the data will be a convolution of information from each pulse in the train. Therefore, an isolated attosecond pulse would be more desirable. It exists two solutions for generating these pulses derived from HHG in gases: using few-cycle pulses and polarization gating. For our system the first solution has been chosen. Fig. 7.6 illustrates the principle of this method. When the incident pulse is short enough, the highest frequency component is generated only at the middle of the pulse, where the intensity is significantly higher than the other part of the pulses. Filtering out that highest frequency part of the spectrum will lead to a single attosecond pulse. When the incident pulse is longer, on the other hand, the high frequency component is generated over several cycles, i.e filtering results in a train of attosecond pulses instead of a single attosecond pulse. It is also important to notice that a shorter incident pulse can lead to a shorter attosecond pulse, because the threshold intensity at the middle will be lower and thus the spectral region that can be used synthesize the attosecond pulse will be broader.

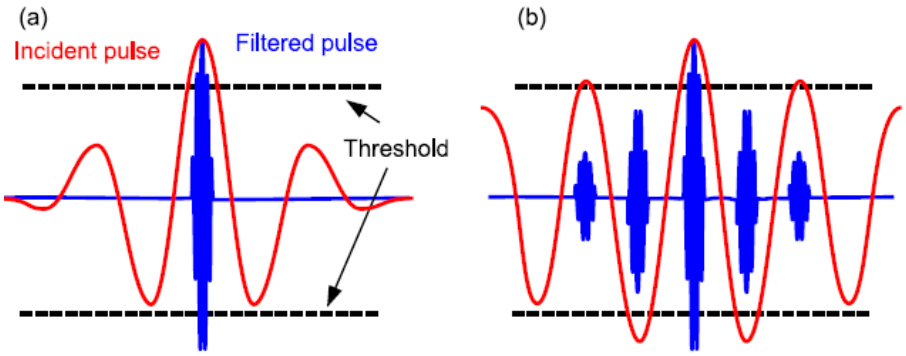

Figure 7.6: Principle of single attosecond pulse generation by a few cycle pulse. Dashed lines show the threshold intensity for generating the high frequency component of interest. (a) When the incident pulse is short, only one cycle contributes to the generation of high frequency component. (b) When the incident pulse is longer, where the high frequency components is generated over several cycles, a train of attosecond pulses is generated instead. These are symbolic drawing to show the idea. In reality, the generation timings of the attosecond pulses do not necessarily coincide the peaks of the field. Reprinted from [17]

It is possible to apply this method to the surface HHG process directly because the principle is the same. There is a small difference that the high frequency components is generated twice per optical cycle for gas HHG, while once per cycle for surface HHG. This difference is actually advantageous in practice because the condition on the pulse duration is slightly relaxed. One important thing to consider is the effect of the carrier envelope phase on the harmonic generation process. In gas HHG, a cosine pulse produces a single attosecond pulse, while a sine pulse produces two attosecond pulses (Fig. 7.7). For surface HHG, numerical simulations predict an analogous behavior. Therefore, as I have already introduced, it is necessary to control the CEP to control the generation of single attosecond pulses.

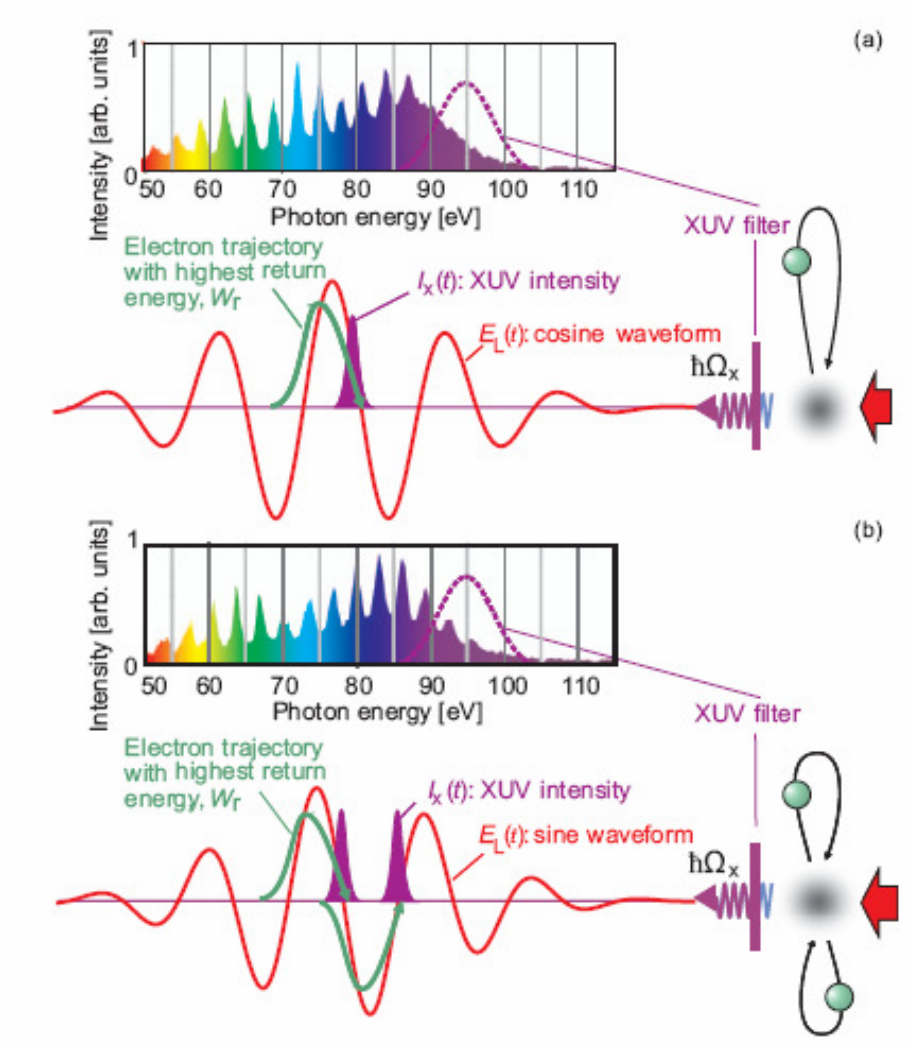

Figure 7.7: High order harmonic spectra obtained experimentally in gases with a few cycle laser. (a) cosine shaped and (b) sine shaped waveform. Reprinted from [13]

7.5 Plasma mirrors

7.5.1 Introduction

I have demonstrated that the "salle noire" laser system satisfies all the initial prescriptions for attosecond generation on solid target. The actual temporal contrast of 7 orders of magnitude in the ns regime is a limitation principally for the ROM harmonics where the highest focused intensity are needed. A solution to increase the temporal contrast without any major modification of the laser system consists of using the plasma mirror technique at the output of the laser. Studying plasma mirror is also very useful because the rotating/translating target for the

plasma mirror is the same that the one used for HHG generation and because this is the first regime of the laser-plasma interaction. Passing from the plasma mirror regime to HHG regime (CWE and then ROM) implies to increase the focused intensity.
Discussing the contrast filtering techniques I have shown that they are based on the nonlinearity on their response. The ionization of a dielectric material, a very nonlinear phenomena, is also a good candidate to be used in a contrast filter. Electric insulators have a large band-gap and are transparent for visible wavelength. However, if the intensity focused on the insulator is sufficiently intense, electrons are excited from the valence band to the conduction band. If the density of the excited electrons is higher than the critical density $N_c = \epsilon_0 m_e \omega_L^2 / e^2$, the dielectric will act like a plasma. In particular it will become highly reflective. The ionization phenomena is also very fast. It can now understood how a plasma mirror works for the contrast enhancement. If the intensity of the pedestal is below the ionization threshold of the target and the main pulse ionizes the target due to multi-photon absorbtion and is reflected, the contrast between the two is increased. This kind of interaction is named plasma mirror. The situation is depicted in Fig. 7.8.

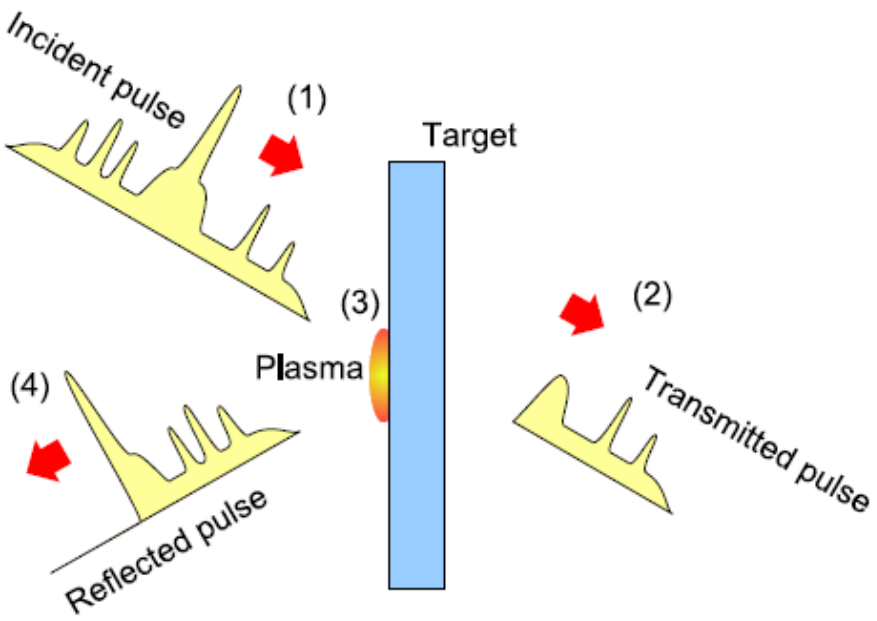

Figure 7.8: Principle of the plasma mirror (1) The incident pulse is focused onto a transparent target. (2) The prepulse/pedestal are transmitted through the material. (3) Plasma is generated by the leading edge of the main pulse. (4) The rest of the pulse is reflected by the generated plasma. Reprinted from [17]

To be more specific, the pedestal, even below the ionization threshold, will be slightly reflected. The contrast enhancement is then the ratio between the initial reflectivity seen by the pedestal and the reflectivity of the plasma generated by the main pulse. It is thus important to limit the initial reflectivity and to have a high plasma reflectivity for the main pulse. Another very important issue is that the plasma generated on the surface of the dielectric will cause a damage in this zone and the next shot needs to illuminate a different point of the target.

This is why, until now, the plasma mirror technique has been applied mainly in single shot configuration or at very low repetition rate. To extent this process to the kHz repetition rate implies working with a rotating and translating target. The development of the target has been done by A. Borot, another PhD member of the PCO group. A representation of the target inside the interaction vacuum chamber is shown in Fig. 7.9.

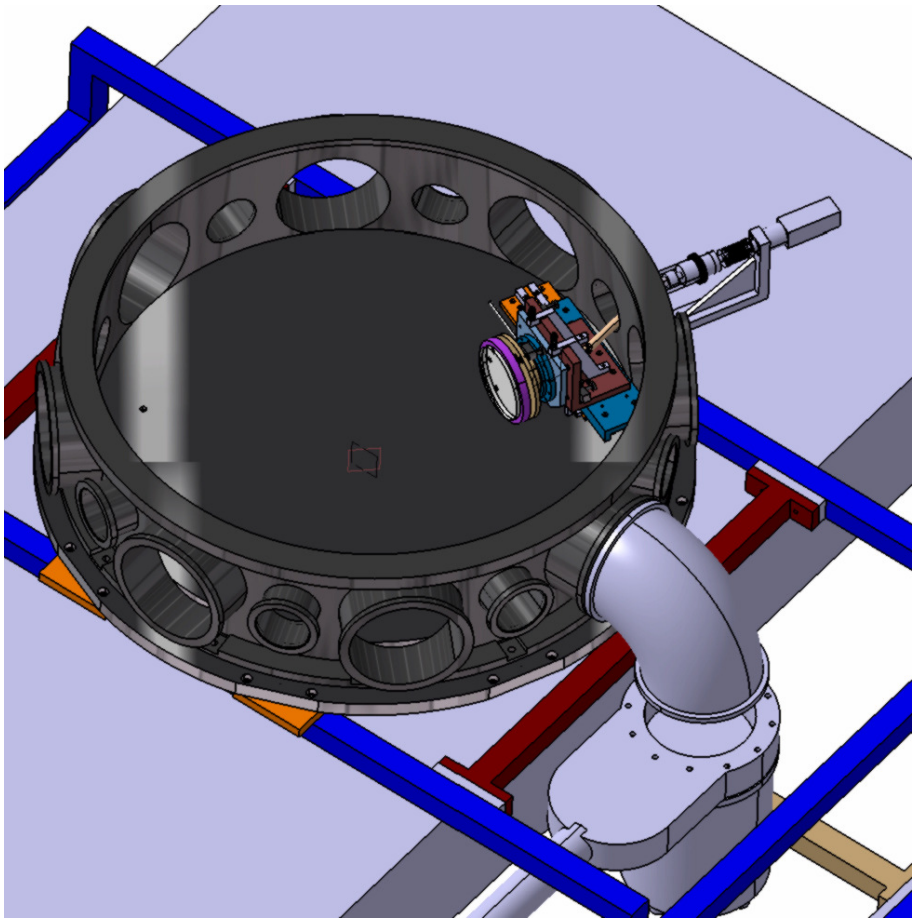

Figure 7.9: Translating/rotating target mounted inside the vacuum chamber. The target is made by fused silica

7.5.2 Experimental setup and results

For the plasma mirror experiments we used the 25 fs pulses compressed with transmission gratings + chirped mirrors. To further clean the spatial profile the output beam passes through the hollow fiber without any gas inside to act just as a spatial filter. The positive dispersion

of the windows is compensated by reflections on the already installed chirped mirrors. The beam is then expanded by a factor of two with a mirror telescope and passes through a $\lambda/2$ and a polarizer. These elements are used to finely tune the fluence on the target. A second $\lambda/2$ is used for changing the polarization state before entering the interaction chamber (under vacuum). Inside the chamber the beam is focused with a f=300 mm lens on the solid target with an incident angle of 45°. This super polished fused silica target has an RMS surface flatness of $\lambda/10$ and an anti reflecting coating at 800 nm.

Fig. 7.10 shows the measured time-and space-integrated reflectivity for s and p polarization function of the input fluence. The maximum fluence corresponds to an input energy of 450 μJ. The input and reflected beam were measured using two calibrated photodiodes and acquired digitally. The fluence is calculated by dividing the input energy by the FWHM of the focused beam which is the same for both polarizations (Fig. 7.11). The highest reflectivity (75 %) is reached with s-polarization. This is due to the absence of the losses due to resonance absorption and Brunel absorbtion [3]. These effects are acting with p-polarization and reduce the reflected energy. On the other hand the reflectivity is higher for s-polarization than for p-polarization (for p-polarization we are close to the Brewster angle).
In s-polarization we expect an increasing of the temporal contrast of 1 order of magnitude with a high transmission efficiency. The contrast enhancement can be increased to 2 orders of magnitude reducing the initial reflectivity with a better anti-reflecting coating.

Generating harmonics after cleaning the temporal contrast with a plasma mirror implies having two rotating targets. Due to the complexity of this setup at the kHz repetition rate and the loss in energy we decided, for the future HHG experiments, to start using the current laser source without any contrast filtering technique. The high contrast ($> 10^{10}$) pulses will be obtained integrating an XPW filter in the laser system in a double CPA configuration. The design of this system is the subject of the next, conclusive chapter.

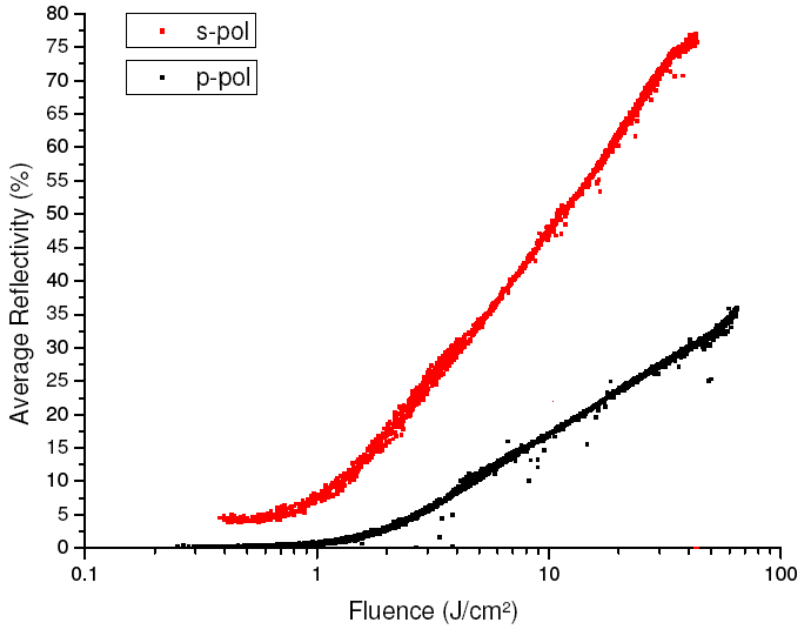

Figure 7.10: Measured time- and space-integrated reflectivity for s and p polarization function of the input fluence. The maximum input energy is 0.45 mJ

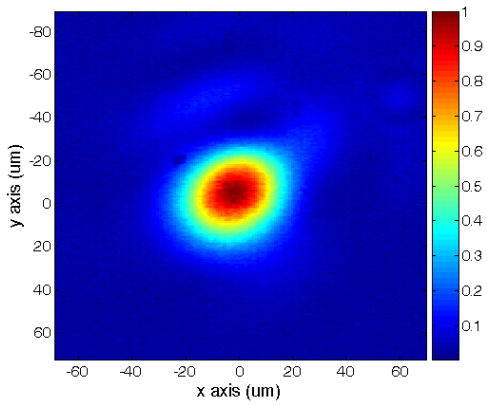

Figure 7.11: Focal spot on the target measured with a CCD camera

Bibliography

[1] T. Baeva, S. Gordienko, and A. Pukhov. Theory of high-order harmonic generation in relativistic laser interaction with overdense plasma. *Physical Review E (Statistical, Nonlinear, and Soft Matter Physics)*, 74(4):046404, 2006.

[2] B. Bezzerides, R. D. Jones, and D. W. Forslund. Plasma mechanism for ultraviolet harmonic radiation due to intense CO_2 light. *Phys. Rev. Lett.*, 49(3):202–205, Jul 1982.

[3] F. Brunel. Not-so-resonant, resonant absorption. *Phys. Rev. Lett.*, 59(1):52–55, Jul 1987.

[4] S. V. Bulanov, N. M. Naumova, and F. Pegoraro. Interaction of an ultrashort, relativistically strong laser pulse with an overdense plasma. *Physics of Plasmas*, 1(3):745–757, 1994.

[5] N. H. Burnett, H. A. Baldis, M. C. Richardson, and G. D. Enright. Harmonic generation in CO_2 laser target interaction. *Applied Physics Letters*, 31(3):172–174, 1977.

[6] R. L. Carman, D. W. Forslund, and J. M. Kindel. Visible harmonic emission as a way of measuring profile steepening. *Phys. Rev. Lett.*, 46(1):29–32, Jan 1981.

[7] R. L. Carman, C. K. Rhodes, and R. F. Benjamin. Observation of harmonics in the visible and ultraviolet created in CO_2 laser-produced plasmas. *Phys. Rev. A*, 24(5):2649–2663, Nov 1981.

[8] B. Dromey, S. Kar, C. Bellei, D. C. Carroll, R. J. Clarke, J. S. Green, S. Kneip, K. Markey, S. R. Nagel, P. T. Simpson, L. Willingale, P. McKenna, D. Neely, Z. Najmudin, K. Krushelnick, P. A. Norreys, and M. Zepf. Bright multi-kev harmonic generation from relativistically oscillating plasma surfaces. *Physical Review Letters*, 99(8):085001, 2007.

[9] G. Farkas and C. Tóth. Proposal for attosecond light pulse generation using laser induced multiple-harmonic conversion processes in rare gases. *Physics Letters A*, 168(5-6):447 – 450, 1992.

[10] P. Gibbon. Harmonic generation by femtosecond laser-solid interaction: A coherent "water-window" light source? *Phys. Rev. Lett.*, 76(1):50–53, Jan 1996.

[11] S. Gordienko, A. Pukhov, O. Shorokhov, and T. Baeva. Relativistic doppler effect: Universal spectra and zeptosecond pulses. *Phys. Rev. Lett.*, 93(11):115002, Sep 2004.

[12] A. Ishizawa, T. Kanai, T. Ozaki, and H. Kuroda. Enhancement of high-order harmonic generation efficiency from solid-surface plasma by controlling the electron density gradient of picosecond laser-produced plasmas. *Quantum Electronics, IEEE Journal of*, 37(3):384–389, Mar 2001.

[13] F. Krausz and M. Ivanov. Attosecond physics. *Reviews of Modern Physics*, 81(1):163, 2009.

[14] R. Lichters, J. Meyer ter Vehn, and A. Pukhov. Short-pulse laser harmonics from oscillating plasma surfaces driven at relativistic intensity. *Physics of Plasmas*, 3(9):3425–3437, 1996.

[15] P. Monot, G. Doumy, S. Dobosz, M. Perdrix, P. D'Oliveira, F. Quéré, F. Réau, P. Martin, P. Audebert, J-C. Gauthier, and J. P. Geindre. High-order harmonic generation by nonlinear reflection of an intensehigh-contrast laser pulse on a plasma. *Opt. Lett.*, 29(8):893–895, 2004.

[16] N. M. Naumova, J. A. Nees, I. V. Sokolov, B. Hou, and G. A. Mourou. Relativistic generation of isolated attosecond pulses in a λ^3 focal volume. *Phys. Rev. Lett.*, 92(6):063902, Feb 2004.

[17] Y. Nomura PhD manuscript

[18] P. A. Norreys, M. Zepf, S. Moustaizis, A. P. Fews, J. Zhang, P. Lee, M. Bakarezos, C. N. Danson, A. Dyson, P. Gibbon, P. Loukakos, D. Neely, F. N. Walsh, J. S. Wark, and A. E. Dangor. Efficient extreme uv harmonics generated from picosecond laser pulse interactions with solid targets. *Phys. Rev. Lett.*, 76(11):1832–1835, Mar 1996.

[19] L. Plaja, L. Roso, K. Rzazewski, and M. Lewenstein. Generation of attosecond pulse trains during the reflection of a very intense laser on a solid surface. *J. Opt. Soc. Am. B*, 15(7):1904–1911, 1998.

[20] F. Quere, C. Thaury, P. Monot, S. Dobosz, Ph. Martin, J.-P. Geindre, and P. Audebert. Coherent wake emission of high-order harmonics from overdense plasmas. *Physical Review Letters*, 96(12):125004, 2006.

[21] Z.-M. Sheng, K. Mima, J. Zhang, and H. Sanuki. Emission of electromagnetic pulses from laser wakefields through linear mode conversion. *Phys. Rev. Lett.*, 94(9):095003, Mar 2005.

[22] A. Tarasevitch, A. Orisch, D. von der Linde, Ph. Balcou, G. Rey, J.-P. Chambaret, U. Teubner, D. Klöpfel, and W. Theobald. Generation of high-order spatially coherent harmonics from solid targets by femtosecond laser pulses. *Phys. Rev. A*, 62(2):023816, Jul 2000.

[23] G. D Tsakiris, K. Eidmann, J. Meyer ter Vehn, and F. Krausz. Route to intense single attosecond pulses. *New Journal of Physics*, 8(1):19, 2006.

[24] K. Varju, Y. Mairesse, Carré B., M. B. Gaarde, P. Johnsson, S. Kazamias, R. Lopez-Martens, J. Mauritsson, K. J. Schafer, PH. Balcou, A. L'huillier, and P. Salières. Frequency chirp of harmonic and attosecond pulses. *Journal of Modern Optics*, 52(2):379–394, 2005.

[25] D. von der Linde, T. Engers, G. Jenke, P. Agostini, G. Grillon, E. Nibbering, A. Mysyrowicz, and A. Antonetti. Generation of high-order harmonics from solid surfaces by intense femtosecond laser pulses. *Phys. Rev. A*, 52(1):R25–R27, Jul 1995.

[26] M. Zepf, G. D. Tsakiris, G. Pretzler, I. Watts, D. M. Chambers, P. A. Norreys, U. Andiel, A. E. Dangor, K. Eidmann, C. Gahn, A. Machacek, J. S. Wark, and K. Witte. Role of the plasma scale length in the harmonic generation from solid targets. *Phys. Rev. E*, 58(5):R5253–R5256, Nov 1998.

Chapter 8

Conclusions and perspective

8.1 Introduction

My Ph.D work focused on the possibility of generating high contrast, ultra-short pulses for doing high repetition rate relativistic optics. In this manuscript I presented the study of the XPW contrast filter for obtaining the high contrast pulses and the development of a mJ level, few-cycle, CEP stabilized source. During this work several devices were developed in collaboration with the company FASTLITE. Two different hybrid compression schemes were tested and the solution based on transmission gratings and chirped mirrors was adapted. Some preliminary results were obtained using the source in laser-matter experiments in the sub-relativistic regime (plasma mirror regime). To efficiently generate harmonics in the relativistic regime a high temporal contrast is also needed. In particular recent experiments underline the importance of a high temporal contrast down to just a few picosecond before the main peak. This implies to control both the incoherent and coherent contrast. The XPW filter is the chosen solution that satisfies those requirements. The installation of a XPW filter in the laser system involves working in a double CPA configuration. The design of this solution is presented in the next sections.

8.2 Double CPA XPW

The front-end of the "salle noire" laser is a commercial system (Femtopower CEP) delivering CEP stabilized, 1 mJ, 30 fs pulses compressed in a prism compressor with a temporal contrast of 10^8. This is the first building block (CPA) of the future system. To generate few-cycle, high contrast pulses there are two possibilities:

- Implement an XPW contrast filter at the output of the Femtopower, seed the second CPA for re-amplification keeping the high contrast. Broaden the spectrum in the hollow-core fiber for the generation of few-cycle (high contrast) pulses. (I)

- Broaden the spectrum to the few-cycle regime in the hollow-core fiber directly after the Femtopower, clean the few-cycle pulses temporally and spectrally with an XPW contrast

filter and seed in the second CPA. (II)

After the developments done during my Ph.D on XPW generation, the two options above are feasible. The second solution is scalable to higher energy but will result in a longer pulse duration due to gain narrowing in the second CPA. Thanks to the XPW spectral cleaning after the hollow fiber, in the second configuration the spectrum will be less modulated but the temporal contrast, at least in the nanosecond regime, will be the same for both configurations (similar injecting energy in the second CPA). The contribution to the coherent contrast due to the residual spectral phase is defined by the second CPA and so should be the same in the two configurations. The contribution due to modulations of the spectrum will be smaller in the second configuration. An experimental implementation similar to the second possibility (except for the XPW filter) has already been tested [2, 3] with the generation of 3.4 mJ pulses with a sub-10 fs temporal duration. Implementing an XPW filter after an hollow fiber with a further amplification in an OPCPA system has also been tested by Tavella et al.

I believe that for our applications the first solution has several advantages in terms of cost, simplicity and robustness. The sensitivity of the XPW filter to the spectral phase has already been demonstrated for sub-10 fs pulses. In terms of daily operation (and also for the need of broadband optics) it is much easier to implement the XPW filter at the 30 fs duration, where the influence of the phase is less critical, followed by pulse broadening in the hollow fiber at the end of the system. This solution is the one designed in the following part.

As I have discussed in section 4.11 the two crystals configuration with the first crystal in focus is not easily scalable to high input energy and short pulse duration. With a reasonable input beam size, in order to avoid white light generation in crystals, a focal length of 10 meter is needed with a distance between the crystals of more than 1 meter to filter 1 mJ, 30 fs pulses (the output of the Femtopower). Furthermore in order to avoid SPM in air, a major part of the setup should be under vacuum. To dispose of a more compact and user-friendly filter there are two solutions:

- the first consists in decreasing the input energy to 200 μJ (with a spatial filter) and work in air with a standard two (holo- cut) crystal setup configuration. In this configuration we have demonstrated the possibility of generating around 50 μJ with a overall efficiency near 30 %. To seed the second CPA the beam needs to be stretched again and eventually passes through another Dazzler. With a 70 % transmission of the stretcher and a 40 % efficiency of the Dazzler there are 17 μJ to be amplified in the second amplifier.

- The second possibility is to try a high energy XPW configuration, using the whole energy and focusing it with a short focal length (1 m) in a vacuum chamber with an iris placed at the focus. The two BaF_2 are placed after the focus where the intensity is below the white light generation threshold. In this configuration a global efficiency (considering also the losses in the iris) of 10 % is expected with an output energy of 100 μJ. The spatial cleaning

in the focus is necessary due to the spatial quality of the beam after the Femtopower. 30 μJ are then injected in the second amplifier. In this case the iris for the spatial filtering and the crystals are placed under vacuum. Due to the limited amount of elements under vacuum a simple plexiglas tube can be used. The advantage of this configuration is its compactness and simplicity of alignment.

The increase in temporal contrast after a XPW filter is determined by the extinction ratio of the polarizers eventually degraded by some linear birefringence of the nonlinear crystals. To be conservative we can consider an increase in temporal contrast of 3 orders of magnitude. Furthermore in both the configurations the spectrum is broadened after the XPW filter and a FWHM >90 nm is expected. Tens of μJ pulses, with a temporal contrast higher than 10^{10} and compressible to 15 fs can then be seeded into the second CPA.
The second amplifier stage has been designed using Commod pro in collaboration with B. Mercier, another member of the PCO group. I assume the pulses stretched to 10 ps. The table with the energy after each pass for the two XPW filter options and for different sizes of the pump beam are shown in Tab. 8.1. This table also gives the accumulated B integral after each pass.

Diameter of the pump spot	800 µm	800 µm	900 µm	900 µm	1 mm	1 mm	
gain per pass	13	13	7.8	7.8	5.2	5.2	
passes	**Energy mJ**						**B integral**
0	0.016	0.032	0.016	0.032	0.06	0.032	radians
1	0.101	0.203	0.072	0.144	0.056	0.113	0.01
2	0.725	1.13	0.351	0.686	0.207	0.409	0.1
3	2.58	3.46	1.3	2.08	0.683	1.2	0.5
4	4.95	5.91	3.04	4.01	1.74	2.57	1.5
5	6.86	7.71	4.85	5.73	3.2	4.09	3.2
6	8.27	9	6.32	7.07	4.59	5.41	5.5

Figure 8.1: amplification for each pass

To obtain the desired energy a 5-pass amplifier is needed. Considering for example a diameter of the pump of 900 μm, pulses with an energy of 4.85 mJ are obtained injecting with 16 μJ (first solution for the XPW filter) and an energy of 5.73 mJ injecting with 32 μJ (second

solution for the XPW filter). The number of passes is limited to 5 to limit the additional B integral to 3.2 rad. The B integral accumulated is the first CPA is cleaned in the XPW filter. As discussed in section 6.3 the Dazscope optimization loop can be used to measure and pre-compensate the additional spectral phase induced by non linear effects during amplification. In the actual configuration of our laser system the stretcher and the compressor are not matched and all the third order spectral phase accumulated in our laser system in compensated by the AOPDF. The pulse can only be stretched to 7 ps and this limit the output energy. Designing the second CPA we can choose a gratings solution both for the stretcher and the compressor and stretch to 10 ps. Using the solution with the hybrid compressor consisting of transmission gratings and chirped mirrors (new grooved gratings with 83 % efficiency), pulses with energies > 3.5 mJ can be obtained and compressed to sub-20 fs. These pulses can then be compressed down to the few-cycle regime in a hollow fiber working with circular polarization. Getting in the few-cycle regime should be facilitated by the short input pulse duration. In section 6.11 I have demonstrated the possibility to generate 1 mJ pulses using a hollow fiber with a diameter of 250 μm. To inject more energy tests are planned using fibers with a 500 μm. The difficulty with a hollow fiber with a big core diameter is keeping a good spatial profile. Another possibility for increasing the input energy of the fibers is the use of a pressure gradient.
The CEP stabilization of the compressed few-cycle pulses at the output of the "salle noire" laser has been demonstrated in section 6.6. The CEP stability directly after the Femtopower has also been presented. The only new element that can affect the CEP stability of the system in the double CPA is the XPW filter. The demonstration that the XPW filter does not introduce significant CEP drift noise into the system is given in the appendix (section 9).

8.3 Conclusion

We can then conclude that, with the design presented in this last chapter, multi-mJ, CEP stabilized, high contrast ($> 10^{10}$), few-cycle pulses can be generated at the kHz repetition rate. A source with these specifications is not currently commercially available but it is realistic to expect that it will be available in the next years due to the importance of its applications. The pulses generated with this source, gently focused on a gaz jet or tightly focused on a solid target, can generate single attosecond pulses. A higher efficiency is expected for the generation on a solid target. The characterization and applications of these attosecond pulses in pump/probe experiments will be the subject of the research for the future years and in particular it will the subject of the experiments with the "Salle Noire" laser system in a near future. Using a deformable mirror to focus these pulses down to the limit of diffraction (λ^2) [1], intensities in the relativistic regime can be obtained and attosecond pulses can be generated with the relativistic oscillating mirror regime or in λ^3 regime. An eventual pre-pulse with controlled amplitude and delay can be added (for example with the AOPDF) to generate a particular plasma density gradient that maximize the harmonic emission.